Dynamic Representation of Taste-Related Decisions in the Gustatory Insular Cortex of Mice

Roberto Vincis[1,3,4,*], **Ke Chen**[1,2,4,*], **Lindsey Czarnecki**[1], **John Chen**[1,2], **Alfredo Fontanini**[1,2,5,*]

[1]Department of Neurobiology and Behavior, Stony Brook University, Stony Brook, NY 11794, USA

[2]Graduate Program in Neuroscience, Stony Brook University, Stony Brook, NY 11794, USA

[3]Department of Biological Science and Program in Neuroscience, Florida State University, Tallahassee, FL 32306, USA

[4]These authors contributed equally

[5]Lead Contact

SUMMARY

Research over the past decade has established the gustatory insular cortex (GC) as a model for studying how primary sensory cortices integrate sensory, affective, and cognitive signals. This integration occurs through time-varying patterns of neural activity. Selective silencing of GC activity during specific temporal windows provided evidence for GC's role in mediating taste palatability and expectation. Recent results also suggest that this area may play a role in decision making. However, existing data are limited to GC involvement in controlling the timing of stereotyped, orofacial reactions to aversive tastants during consumption. Here, we present electrophysiological, chemogenetic, and optogenetic results demonstrating the key role of GC in the execution of a taste-guided, reward-directed decision-making task. Mice were trained in a two-alternative choice task, in which they had to associate tastants sampled from a central spout with different actions (i.e., licking either a left or a right spout). Stimulus sampling and action were separated by a delay period. Electrophysiological recordings revealed chemosensory processing during the sampling period and the emergence of task-related, cognitive signals during the delay period. Chemogenetic silencing of GC impaired task performance. Optogenetic silencing of GC allowed us to tease apart the contribution of activity during sampling and delay periods. Although silencing during the sampling period had no effect, silencing during the delay period significantly impacted behavioral performance, demonstrating the importance of the cognitive signals processed by GC in driving decision making. Altogether, our data highlight a novel role of GC in controlling taste-guided, reward-directed choices and actions.

In Brief

Relying on behavioral electrophysiology and neural manipulations, Vincis, Chen, et al. demonstrate that neurons in the gustatory cortex (GC) encode perceptual and cognitive signals important for tasteguided choices. These data demonstrate a novel role of GC as a key area for sensorimotor transformations related to gustatory perceptual decision making.

INTRODUCTION

The gustatory cortex (GC), a subregion of the insular cortex, has traditionally been investigated for its function in processing taste identity [1]. In the past decade, studies in alert animals significantly changed the classic view of this area, establishing a role for GC in dynamically representing affective, multisensory, and cognitive signals associated with the experience of eating [2–4]. Time-varying patterns of firing activity in GC are important for the perception and learning of taste value [5–7], for multisensory integration in the context of flavor and taste expectation[8–12],and for guiding food-directed behaviors on the basis of food-predictive cues [13–15].

Recent experiments indicated that GC may also be involved in mediating decisions based on gustatory cues. Electrophysiological recordings and optogenetic manipulations in rats consuming tastants demonstrated that GC activity is instructive of ingestive decisions [16]. Indeed, sudden changes in ensemble activity occurring during the time course of a response correlated with and determined the onset of gapes—aversive reactions aimed at expelling highly unpalatable tastants [16]. The function of GC is not limited to naturalistic consummatory decisions involving stereotyped, orofacial reactions to aversive tastants. Single-unit recordings in an operant task classically used to study perceptual decision making (i.e., a taste-based, two-alternative choice task [2-AC]) suggested that neurons in GC may encode taste-guided, reward-directed choices and actions [17]. However, the extent to which activity in GC contributes to driving reward-directed choices in a 2-AC task is currently unknown. Furthermore, it is not established whether GC contributes to decision making by exclusively representing chemosensory information (i.e., sensory evidence necessary for decisions) or by encoding also cognitive variables, such as planning for specific behavioral choices and actions.

In this study, we addressed these unresolved issues by recording and manipulating GC activity in the context of a taste-based, two-alternative choice task optimized for the investigation of sensory and task-related variables. We designed a 2-AC task in which pairs of gustatory stimuli of opposite perceptual and hedonic categories (sweets and bitters) sampled from a central spout were rewarded with water delivered at two lateral spouts. The task featured a delay period,specifically introduced to better resolve activity-anticipating decisions and actions [18]. We recorded GC neurons' spiking activity in well-trained, head-restrained mice. Analysis of single-unit and population activity revealed a progression from chemosensory coding to the representation of task-related variables. Specifically, we observed that GC neurons encode information about the action-predictive value of tastants and about planning of an imminent behavioral choice during the delay period. The behavioral significance of this task-related activity was validated with optogenetic silencing

of GC, which demonstrated that interfering with activity during the delay epoch, but not taste sampling, significantly reduced behavioral performance.

Our results show that GC neurons dynamically encode multiple variables associated with a perceptual decision-making task and demonstrate that activity during the period preceding a taste-guided, reward-directed choice is instructive of behavior. This evidence significantly changes our understanding of the function of GC in taste, demonstrating its role as a key node for gustatory decision making.

RESULTS

Performance in a Taste-based, 2-AC Task

We trained head-restrained mice to perform a taste-based 2-AC (Figure 1) task. In a taste-based 2-AC task, mice learn to sample tastants by licking a central spout (only one stimulus is presented at each trial) and respond to each stimulus according to a specific policy (e.g., taste A → lick a left spout or taste B → lick a right spout). The policy is reinforced by rewarding correct responses with water deliveries. We chose this task because it engages multiple sensory and cognitive processes. Mice must identify the sensory quality of each gustatory stimulus delivered at the central spout, correctly interpret its predictive value, plan a response, and act. In our version of the task, sensation (i.e., sampling of taste stimuli from the central spout) and action (i.e., lick the left or right spout for reward) were separated by a delay epoch (~2 s; Figure 1B) in order to facilitate the study of sensory and cognitive processes. For this study, mice were trained to sample 2 μL of one out of four taste stimuli (sucrose [100 mM], quinine [0.5 mM], maltose [300 mM], and sucrose octaacetate [0.5 mM]) delivered from the central spout at each trial and to associate pairs of tastants with the different actions (Figures 1A and 1B). After a delay epoch initiated by the retraction of the central spout, two lateral spouts advanced and mice could lick toward the left or right lateral spout to receive a small drop of water reward (3 μL). Mice were trained to associate sucrose (S) (sweet and palatable) and quinine (Q) (bitter and aversive) with reward from the left spout and maltose (M) (sweet and palatable) and sucrose octaacetate (SO) (bitter and aversive) with reward from the right spout. In this configuration, each action (left or right lick) was paired with two tastants with opposite hedonic value and different taste quality (e.g., S or Q → lick left spout; M or SO → lick right spout), rendering mice unable to solve the task by simply generalizing for taste palatability or quality.

Upon learning the task, mice showed no bias in the performance. The average duration of the sampling (i.e., the time during which a mouse licked the central spout to sample the tastant) was 0.50 ± 0.02 s, and the average licking frequency was 8.65 ± 0.16 Hz. No significant difference in sampling duration or licking frequency was observed for the four tastants (n = 16; one-way ANOVA; for sampling duration, $F_{(3,60)} = 0.12$, $p = 0.94$, Figure 1C; for licking frequency, $F_{(3,60)} = 0.04$, $p = 0.99$). The reaction time for left trials (measured as the interval between the last lick for the central spout and the first lick for a lateral spout) was comparable to that for right trials (n = 16; 2.02 ± 0.04 s versus 1.95 ± 0.03 s; paired t test; $t_{(15)} = 1.59$; $p = 0.13$; Figure 1D), and mice showed similar licking duration and frequency to each lateral spouts (n = 16; left versus right; duration: 1.04 ± 0.03 s versus 0.97 ± 0.06 s, paired t test, $t_{(15)} = 1.03$, $p = 0.32$, Figure 1E; frequency: 7.22 ± 0.15 versus

7.44 ± 0.38 Hz, paired t test, $t_{(15)} = 1.61$, $p = 0.13$), indicating lack of any lateral bias. Finally, mice showed similar behavioral performance for each of the four tastants (n = 16; one-way ANOVA; $F(3,60) = 1.5$; $p = 0.22$; Figure 1F), denoting that they could learn the contingency for each tastant and further confirming the absence of any bias toward one or more specific tastants used in the task.

Taste Classification during Sampling and Delay Epochs

Single-unit spiking activity was recorded with movable bundles of 8 tetrodes unilaterally implanted in GC of mice performing the 2-AC task at criterion (Figure S1A). Neural activity, licking activity, as well as orofacial movements were simultaneously recorded. Given the involvement of GC in representing taste [19, 20], we first analyzed activity evoked by S, Q, M, and SO during the sampling epoch. Spiking activity was aligned to the first lick at the central spout (time 0; detection of the taste; Figure 2A) and analyzed for a 500-ms temporal window (sampling epoch; Kruskal-Wallis test; $p < 0.05$; Figure 2A). As expected, a sizable portion of GC neurons changed their firing rate following the licking of a gustatory stimulus and had significantly different responses to the four tastants (Figure 2B). Specifically, we observed that 33.6% (72/214) of recorded neurons were modulated by at least one of the four tastants (Figure 2C). Of these taste-responsive neurons, 73.6% (53/72) were modulated by S, 63.8% (46/72) by Q, 84.7% (61/72) by M, and 66.7% (48/72) by SO (Figure 2D).

Gustatory processing in GC is dynamic, and evidence from the literature suggests that responses may persist or emerge beyond the initial 500-ms sampling epoch [6]. To begin assessing the temporal dynamics of gustatory processing, we performed a population-decoding analysis across sampling and delay epochs [21] (decoding was based on maximum correlation coefficient; see STAR Methods). We found that taste decoding was more accurate in the sampling epoch (0–0.5 s) compared to the later part of the delay epoch (1.5–2.5 s), indicating that taste decoding accuracy slightly decays during the delay (n = 181; see STAR Methods; decoding accuracy: 0.61 ± 0.01 in sampling epoch, 0.59 ± 0.01 and 0.57 ± 0.01 in the delay epoch; one-way ANOVA, $F(2,27) = 4.8$, $p = 0.016$; post hoc Tukey's HSD test, $p < 0.05$; Figure 2E). In addition, we constructed confusion matrices for population decoding and characterized the classification performance for each taste. We found that, compared to the sampling epoch or the first part of the delay (0.5–1.5 s), the decoder made more mistakes between tastants associated with the same actions (i.e., S and Q trials or M and SO trials; permutation test; $p < 0.001$; see STAR Methods) in the later part of the delay (1.5–2.5 s; Figure 2F). This observation suggests that neural activity evoked by tastants associated with the same action converges during the second half of the delay epoch. To visualize temporal dynamics of population activity, we applied a principal-component analysis (PCA) (Figure 2G). Visual inspection of the trajectories of taste-evoked temporal dynamics reveals that S- and Q-evoked activity converged to the same small region in the PC space in the late phase of the delay (blue spot, Figure 2G) and that M- and SO-evoked activity converged to a distinct spot in the PC space (red spot, Figure 2G). The Euclidean distance in PC space between S- and Q-evoked activity or between M- and SO-evoked activity gradually decreased in the delay epoch (0.52.5 s; Figure 2H). To confirm that activity becomes more similar for pairs of tastants associated with the same actions, we

computed the pairwise distance in normalized firing rates evoked by each taste for each neuron (n = 214; see STAR Methods). The distance for firing activity evoked by pairs of tastants associated with the same actions gradually decreased—reflecting an increase in the similarity of the responses. In contrast, the distance for pairs of tastants associated with the same taste quality and hedonic value (sweets and palatable [S and M] versus bitter and aversive [Q and SO]) gradually increased (Figure 2I).

Altogether, these data demonstrate that, in the context of a perceptual decision-making task, taste processing is not restricted to the sampling epoch but continues throughout the delay period and that GC categorizes tastants according to different criteria in different epochs. As time progresses, GC shifts from coding the chemosensory identity of tastants to firing more similarly for stimuli anticipating the same action.

Action-Related Activity in the Delay Epoch

To further investigate neural activity during the delay epoch and identify neurons responsible for the changes seen in confusion matrices and pairwise distances, we compared each neuron's firing rates in anticipation of correct left or correct right licking. Consistent with previous literature, we computed a direction index using a receiver operating characteristic (ROC) analysis (see STAR Methods) [17, 22]. A large group of neurons (41.6% of all recorded neurons; 89/214) showed a direction index significantly different from 0 (i.e., having a significant lateral bias) during the delay epoch (permutation test; $p < 0.01$; see STAR Methods; Figure 3B), with 57.3% (51/89) and 42.7% (38/89) of neurons showing higher firing rates in anticipation of leftward and rightward licking, respectively (Figures 3C and 3D; see also Figures S2A and S2B for an alternative analysis of direction preference). Figure 3B shows raster plots and peristimulus time histograms (PSTHs) for two representative neurons, one with higher firing rate during the delay epoch in left trials (neuron no. 1) and the other showing higher firing rate for right trials (neuron no. 2). Direction selective firing could begin at any time during the delay period—i.e., from 2 s prior to the moment of the lateral lick—as shown in the color-coded population PSTH in Figure 3D. Inspection of the average direction index (white traces superimposed to the color plot in Figure 3D) revealed that direction selectivity peaks right before the animal licks the lateral spouts.

To determine whether these direction-selective neurons carried information regarding the chemosensory identity (sweet versus bitter) of specific tastants, we compared firing rates for S versus Q trials (left trials) or for M versus SO trials (right trials; Figures 3E and S2C). We found that 38.2% (34/89) of the neurons with a direction index significantly different from 0 also showed significant taste selectivity during the delay epoch (permutation test; $p < 0.01$; see STAR Methods; Figure 3F, gray dots). Plot of the maximum value for taste selectivity against the absolute value of the direction index revealed that the activity of the majority of neurons, 74.1% (66/89), was more strongly modulated by the anticipated direction of licking than by the chemosensory identity of the tastant (Figure 3F). This bias was specific to the delay period, as the same analysis performed for the sampling period revealed that the majority of neurons (80.9% [72/89]) were more strongly modulated by taste compared to the anticipated licking direction (Figure S2D).

In principle, direction-selective activity could be evoked either by the tastants (and reflect taste recategorization according to each stimulus' predictive value), by internal signals pertaining to the preparation/planning of a specific action, or by a combination of both. To investigate these possibilities, we analyzed responses for correct and error trials for the same pairs of cues (e.g., correct: S and Q → left lick; error: S and Q → right lick). If GC was involved exclusively in taste recategorization, activity would depend just on gustatory cues, hence failing to differentiate error and correct trials. On the contrary, delay activity related to action planning would allow for the classification of correct and error trials for the same gustatory cues. A decoding analysis (Figure 3G) revealed that the delay activity in the population of neurons with direction selectivity can indeed differentiate between correct and error trials (i.e., distinguishing left-cued correct trials from left-cued incorrect trials and right-cued correct trials from right-cued incorrect trials). Classification of correct and errors peaked short after the action (peak accuracy = 0.94; 0.25 s after lateral licking) but was already significant in the delay period (-0.5–0 s; permutation test with $p < 0.001$). This classification performance was related to neurons with comparable direction index, regardless of the gustatory cue (gray shading in Figure 3H), like the one shown in Figure 3I. Not all direction-selective neurons behaved like the one in Figure 3I. Some neurons represented pairwise similarities between S and Q (or M and SO), regardless of action (unshaded area in Figure 3H and Figure S2E), indicating that GC can also represent taste recategorization and hence adopt a mixed coding scheme.

Preparatory activity and direction selectivity in the delay epoch may be related to orofacial movements. To investigate this relationship, we analyzed videos of the orofacial region during the entire delay period (Video S1). Visual inspection of traces extracted from the video analysis (Figures S3B–S3D) suggests that, despite the directionality of tongue protrusions at the end of the delay epoch (see below), the magnitude of preparatory movements during the entire delay epoch was similar for left and right trials. ROC analysis confirmed that orofacial activity in left and right trials averaged across the entire delay period was comparable for all the sessions analyzed (Figure S3E). Furthermore, inspection of traces for neural and orofacial activity suggests that the onset of delay activity preceded the onset of preparatory movements (Figure S3C). We performed additional video analysis to quantify the time course of preparatory lateral movements unique to each outcome (Figure S3F). On average, mice produced choice specific, preparatory tongue protrusions only 200 ms prior to licking the lateral spout, which is well after the onset of preparatory neural activity. Thus, it is unlikely that the patterns of neural activity observed during the delay epoch can be exclusively accounted by overt differences in orofacial movements visible from our video analysis.

Altogether, the results reveal that, during the delay epoch, a large fraction of GC neurons can show firing rate modulations in anticipation of a specific licking direction. At the population level, delay activity can differentiate between correct and error trials—a pattern that is consistent with action preparation and planning. In addition, a portion of neurons with direction selectivity can encode taste and taste recategorization. Together, these findings confirm the existence of task-related activity during the delay period and suggest that GC multiplexes information related to taste recategorization and action planning.

Involvement of GC in the Performance of a Taste-Based 2-AC Task

Recent experimental evidence highlights that neural activity recorded in multiple brain regions, including sensory and motor cortices, correlates with movement and goal-directed behavior [23–25]. However, not all areas are instrumental for performing the task [25]. To evaluate whether the modulation of activity described above is necessary to optimally perform a taste-based 2-AC task, we silenced the GC using two experimental strategies. First, we adopted a chemogenetic approach. Adeno-associated viral (AAV) constructs (AAV8-hSyn-hM4DimCherry) carrying the inhibitory Gi-DREADD (hM4Di) were bilaterally injected into GC (Figures 4A and S1B). Neurons expressing hM4Di can be silenced by clozapine N-oxide (CNO) [26]. In our experimental conditions, intraperitoneal injection of CNO (10 mg/kg) significantly impaired behavioral performance (fraction of correct trials; saline versus CNO: 0.82 ± 0.02 versus 0.69 ± 0.03; two-way ANOVA; main effect: CNO application, $F(1,9) = 6.93$, $p = 0.027$; interaction: $F(1,9) = 4.70$, $p = 0.06$; post hoc Bonferroni's multiple comparisons test, adjusted $p = 0.01$; Figure 4B, left panel). In contrast, CNO did not affect the performance in a separate group of mice that received an injection of a control viral construct (AAV8-hSyn-mCherry) lacking the inhibitory Gi-DREADD (CNO versus saline; 0.80 ± 0.02 versus 0.79 ± 0.02; two-way ANOVA; main effect: CNO application, $F(1,9) = 6.93$, $p = 0.027$; interaction: $F(1,9) = 4.70$, $p = 0.06$; post hoc Bonferroni's multiple comparisons test, adjusted $p > 0.99$; Figure 4B, right panel). In neither Gi-DREADD nor control mice, CNO injection affected sampling duration or reaction times (Figures S4A and S4B). These results indicate that GC activity is required to perform a taste-based 2-AC task.

GC could be involved in mediating the performance of a 2-AC task for either its role in representing taste identity—a process predominantly happening during the sampling epoch —or for its ability to process task-related variables, such as recategorization of tastants and action planning—both occurring during the delay epoch. To investigate this, we employed an optogenetic approach to transiently inhibit the GC during different epochs. AAV constructs (AAV5-EF1α-DIO-ChR2-EYFP) carrying Cre-dependent channelrhodopsin-2 (DIO-ChR2) were injected bilaterally into the GC of PV-Cre mice, resulting in the expression of ChR2 in parvalbumin (PV)-expressing inhibitory neurons (Figures 4C and S1C). Optical stimulation of PV neurons is widely used to inhibit cortical circuits [18, 27– 29]. Bilateral photoactivation of PV neurons in GC over the sampling epoch did not significantly affect task performance (no stimulation [none] versus light stimulation [light]; 0.77 ± 0.01 versus 0.74 ± 0.02; two-way ANOVA; main factor: light stimulation, $F(1,21) = 0.17$, $p = 0.68$; interaction: $F(1,21) = 2.30$, $p = 0.14$; Figure 4D) or sampling duration and reaction time (Figures S4D and S4E). In contrast, activation of GC PV neurons during the delay epoch significantly reduced the performance (no stimulation [none] versus light stimulation [light]; 0.78 ± 0.01 versus 0.64 ± 0.02; two-way ANOVA; main factor: light stimulation, $F(1,22) = 11.69$, $p = 0.003$; interaction: $F(1,22) = 14.03$, $p = 0.001$; post hoc Bonferroni's multiple comparisons test, adjusted $p < 0.001$; Figure 4E) and slightly increased reaction time (no stimulation [none] versus light stimulation [light]; 1.96 ± 0.02 versus 2.03 ± 0.02 s; two-way ANOVA; main factor: light stimulation, $F(1,22) = 8.09$, $p = 0.01$; interaction: $F(1,22) = 7.08$, $p = 0.01$; post hoc Bonferroni's multiple comparisons test, adjusted $p = 0.002$; Figure S4H). In a second group of PV-Cre mice, where only EYFP was

expressed in GC PV neurons, there was no change in performance following light stimulation during either the sampling or the delay epoch (sampling epoch: 0.82 ± 0.02 versus 0.83 ± 0.01; two-way ANOVA; main factor: light stimulation, $F_{(1,21)} = 0.17$, $p = 0.68$; interaction: $F_{(1,21)} = 2.30$, $p = 0.14$; delay epoch: 0.83 ± 0.01 versus 0.85 ± 0.02; two-way ANOVA; main factor: light stimulation, $F_{(1,22)} = 11.69$, $p = 0.003$; interaction: $F_{(1,22)} = 14.03$, $p = 0.001$; post hoc Bonferroni's multiple comparison test, adjusted $p > 0.99$; Figures 4D and 4E).

Altogether, these results demonstrate that GC is required for properly performing a taste-based 2-AC task and that task performance is affected by optogenetic manipulation during the delay period, but not during the sampling epoch.

DISCUSSION

The results presented here demonstrate that GC is one of the sites of sensorimotor transformations related to taste-guided, reward-directed decision making. We trained mice in a taste-based 2-AC task. Subjects had to sample from a central spout one out of four tastants (S, Q, M, and SO) randomly selected at each trial, wait during a delay period, and respond by licking one of two lateral spouts. Mice were trained to lick left in response to S and Q or right in response to M and SO; correct responses were rewarded with water. We used four stimuli to make the task more challenging and to facilitate the analysis of sensory-related signals. Furthermore, by having a sweet, palatable stimulus (S or M) and a bitter, aversive stimulus (Q or SOA) associated with the same response, we prevented mice from simplifying the task into a discrimination of two predetermined gustatory or hedonic categories (sweets versus bitters). The separation of sampling, delay, and response in distinct epochs allowed us to study the temporal evolution of neural activity and its relationship to the task. We found that GC neurons represent gustatory information and task-related variables. Taste processing was not limited to the sampling epoch but continued throughout the delay period, shifting from representing the chemical identity of tastants to representing their predictive value (lick left or right). This change in similarity of responses to S, Q, M, and SO is consistent with the notion that GC dynamically recategorizes tastants according to the action they predict. Analysis of activity during the delay epoch showed that, in addition to processing taste, GC neurons modulated their firing in anticipation of a licking direction, with some neurons selectively anticipating either left or right licks. Decoding analysis of correct and error trials revealed that activity in GC was not just linked to taste recategorization. Responses to the same tastants differentiated correct from error trials during the delay epoch. This result is consistent with delay activity representing action preparation and planning, albeit we do not exclude that variability in the representation of taste categories may also partly account for differences in correct and error trials. Altogether, these recordings show that, although activity in the sampling period is mostly linked to chemosensory processing, activity in the delay period reflects sensorimotor transformations based on recategorization of gustatory cues and preparation for a specific behavioral response. To test for the behavioral role of GC and its neural activity during the different epochs, we relied on chemogenetic and optogenetic manipulations. Silencing of GC with inhibitory DREADD led to a reduction in the overall performance, with fewer correct responses. Temporally restricted optogenetic activation of GABAergic neurons demonstrated

that perturbation of GC activity during the delay period significantly reduced task performance, although interfering with activity during the sampling epoch had no visible impact on behavior. Taken together, we demonstrated that the contribution of GC in a decision-making task is largely due to the integration of perceptual and cognitive signals rather than just sensory processing. This result goes against classic views of cortical taste processing and emphasizes the role of GC in driving behavior.

Temporal Dynamics in GC

A well-established model of taste processing posits that GC represents taste through time-varying modulations in spiking activity. In its original instantiation, this model describes the evolution of taste responses through three distinct temporal epochs unfolding over a few seconds from the delivery of a tastant [6]. The first epoch (somatosensory) lasts a few hundred milliseconds after stimulus onset and corresponds to the general tactile sensation of tastants contacting the tongue. The second epoch (chemosensory) starts after the first, lasts about 1 s, and corresponds to a phase in which taste qualities are maximally differentiated. The third epoch (palatability) begins about 1 s after stimulus delivery and relates to the processing of taste palatability. This coding scheme has been further refined through trial-by-trial ensemble analyses and has been extensively validated by experimental evidence in rats and mice [5, 7, 16, 30, 31]. Alas, one of the limitations of this model has been its exclusive reliance on experiments in which rodents consume tastants that are flushed directly into the oral cavity through a surgically implanted intraoral cannula. Our experiments demonstrate that temporal multiplexing can be observed also in the context of mice engaged in a decision-making task that relies on licking. We observed that chemosensation gave way to recategorization and action planning as activity progressed from the sampling through the delay epoch. Taste recategorization consisted in shifting the pairwise representation of tastants toward similarities in predicted actions (lick left versus lick right). Planningrelated signals consisted in activity that was predictive of the same licking direction, regardless of the gustatory cue. Recategorization and planning were not isolated in different temporal windows but rather intertwined during the delay epoch, suggesting that perceptual and decisional processes do not segregate in time. It is worth noting that this dynamic processing was not achieved through the activation of mutually exclusive neurons, as the same units could process multiple sensory and task-related variables (Figure S2F). This result argues against the existence of cognitive labeled lines in GC. Furthermore, the convergence of perceptual and preparatory activity onto the same neurons in the same epoch, together with the diversity of responses at correct and incorrect trials, may also be interpreted as evidence for a unitary process of sensorimotor transformation rather than two distinct sensory and preparatory processes.

In summary, our results demonstrate that, although the specific temporal structure and the variables encoded in GC firing rates may vary from task to task, and depending on experimental conditions, the temporal multiplexing of sensory and cognitive signals is a fundamental mode of function of GC.

Functional Role of GC

GC has been implicated in multiple functions related to taste processing, taste learning, and taste expectation [1, 11, 32, 33]. Recent evidence also suggests that GC can be involved in taste-based decision making [16, 17]. Recordings from GC of rats consuming tastants delivered through an intraoral cannula demonstrate that sudden and coherent changes in ensemble activity predict gapes—an innate orofacial behavior aimed at expelling aversive tastants [16]. Optogenetic experiments, showing that perturbation of GC activity prior to ensemble transitions delays the onset of gapes, confirm the importance of this area in driving this ingestive decision. Although important and novel, the work described above has focused exclusively on innate, ingestive responses evoked by aversive stimuli. A recent set of electrophysiological experiments relied on a 2-AC task to investigate GC activity related to decision making in the context of a structured, reward-oriented paradigm [17]. Although GC showed patterns of activity consistent with decision making, it appeared less engaged by the task than the orbitofrontal cortex, raising the possibility that task-related activity might be epiphenomenal in GC. Evidence in the rodent's brain of global preparatory signals [25] that are not necessarily instructive of behavior further raises questions on the role of reward-related, decision-making activity in GC. Our experiments were explicitly designed for an in-depth investigation of patterns of firing activity associated with a 2-AC task and for a test of their behavioral significance. The reliance on restrained subjects and the use of a delay period before the decision allowed us to record task-related signals in the absence of overt movements associated with a 2-AC task in freely moving rodents. Video analysis of orofacial movements suggested that the task-related signals observed here were not simply driven by visible mouth movements preceding and unique to future left or right licking. Chemo- and optogenetic experiments ultimately confirmed the hypothesis that activity during the delay was instructive of task performance and not epiphenomenal. Indeed, manipulation of GC activity unveiled a role for GC activity in the 2-AC task. Chemogenetic silencing resulted in a significant reduction of performance, pointing at GC playing a role in the execution of the task. Temporally restricted optogenetic perturbation of GC (through activation of PV-positive GABAergic neurons) allowed us to investigate the contribution of GC activity in different epochs, parsing apart the role of sensory and task-related signals. Optogenetic manipulation around the sampling epoch—a time in which chemosensory processing occurs with little or no cognitive signaling—had no impact on behavioral performance. On the contrary, perturbation during the delay epoch—a window during which we observed firing related to taste recategorization and licking direction planning— significantly reduced the performance.

The lack of behavioral effect of optogenetic perturbation at sampling may appear puzzling at first. How can GC perform its role in decision making and sensorimotor transformation without sensory information? Sampling-related activity within GC may not be the only source of gustatory information for computations occurring during the delay epoch. Indeed, subcortical nuclei relaying gustatory signals to the cortex process taste with changes in firing activity that persist longer than 500 ms [34, 35]. Hence, it is conceivable that, despite the temporary perturbation of intracortical activity at sampling, during the delay period, the thalamus and parabrachial nucleus (and other sources of gustatory information) may provide GC with the signals necessary for performing sensorimotor computations. Of course, other

possible explanations should be considered. For instance, it is possible that, in highly trained animals, GC may not be necessary for discriminating tastants or that taste processing in GC may be more robust to perturbation than task-related signals. Regardless of the reason for this surprising result, the ineffectiveness of optogenetic manipulation during the sampling epoch indicates that the contribution of GC to a taste-based, 2-AC is not in merely detecting gustatory stimuli at the time of licking. Instead, our results point at the importance of the integration of perceptual (recategorization) and cognitive (planning) activity during the delay epoch for reward-related licking decisions. Future studies will have to address how and through what mechanisms GC comes to express these patterns of activity during learning. It is possible that the signals that we observed may emerge through interaction with amygdala, orbitofrontal cortex, and motor cortices. Although the exact contribution of these areas is a matter of speculation, it is tempting to propose that amygdala and orbitofrontal cortex may contribute to the formation of taste-action associations, taste recategorization, and to the resolution of palatability conflicts for tastants associated with the same action. As for the role of motor cortices, although direct connections between GC and motor cortices are not well documented, it is possible that indirect interactions may be important for the genesis of preparatory activity. Of course, we cannot exclude that local computations in GC may play themselves a fundamental role in decision making.

Regardless of these mechanistic issues, the data presented here demonstrate that the function of GC goes beyond chemosensory processing and beyond controlling the timing of naturalistic, aversive reactions, as it is also the site of taste-guided, reward-related decision making.

STAR★METHODS

LEAD CONTACT AND MATERIALS AVAILABILITY

Further information and requests for resources and reagents should be directed to and will be fulfilled by the Lead Contact, Alfredo Fontanini (alfredo.fontanini@stonybrook.edu). This study did not generate new unique reagents.

EXPERIMENTAL MODEL AND SUBJECT DETAILS

Experiments were performed on 24 adult male mice (10–20 weeks old). Only male mice were used to limit the potential variability that may be introduced by estrous cycle in female mice. Sixteen C57BL/6 mice (Charles River) were used for electrophysiological recordings and chemogenetic experiments. Eight PV-Cre mice (The Jackson Laboratory, Stock # 017320) were used for optogenetic experiments. Mice were group housed and maintained on a 12 h light/dark cycle with ad *libitum* access to food and water unless otherwise specified. All experimental protocols were approved by the Institutional Animal Care and Use Committee at Stony Brook University, and complied with university, state, and federal regulations on the care and use of laboratory animals.

METHOD DETAILS

Adeno-associated viral constructs—For chemogenetic experiments, we used the following viral constructs: AAV8-hSyn-hM4Di-mCherry (7.4×10^{12} vg/ml, UNC vector

core or Duke Viral Vector Core) and AAV8-hSyn-mCherry (2×10^{13} vg/ml, Duke Viral Vector Core). For optogenetic experiments, we used AAV5-EF1α-double floxed-hChR2(H134R)-EYFP-WPRE-HGHpA (7.7×10^{12} vg/ml, Addgene, catalog #: 20298-AAV5) and AAV5-EF1α-DIO-EYFP (1.3×10^{13} vg/ml, Addgene, catalog #: 27056-AAV5).

Surgical procedures for viral injections, fiber optic cannulae and electrodes implantation—Mice were anesthetized with an intraperitoneal injection of a cocktail of ketamine (70 mg/kg) and dexmedetomidine (1 mg/kg). Once fully anesthetized, they were placed on a stereotaxic apparatus. The depth of anesthesia was monitored regularly via visual inspection of breathing rate, whisking and by periodically assessing the tail reflex. A heating pad (DC temperature control system, FHC, Bowdoin, ME) was used to maintain body temperature at 35°C. Once a surgical plane of anesthesia was achieved, the animal's head was shaved, cleaned and disinfected (with iodine solution and 70% alcohol) and fixed on a stereotaxic holder. For viral injections, a small craniotomy was bilaterally drilled above GC (AP: +1.2 mm, ML: ± 3.5 mm relative to bregma). A pulled glass pipette front-loaded with the viral constructs was lowered into GC (−2.0 mm from brain surface). 100–150 nL of virus was injected at 1 nl/ s with a microinjection syringe pump (UMP3T-1, World Precision Instruments, Sarasota, FL). Following injection, we waited additional 5 minutes before slowly pulling the pipette out. For optogenetic experiment, two tapered fiber optic cannulae [36] (Ø 200 μm core, emitting length = 1 mm, NA = 0.39, Optogenix, Lecce, Italy) were slowly lowered into GC (−1.85 mm from the brain surface) after virus injections (Figure S1C). For electrophysiological experiments, craniotomies were opened above the left GC (AP: 1.2 mm, ML: 3.5 mm relative to bregma) and above the visual cortex for implanting movable bundles of 8 tetrodes (Sandvik-Kanthal, PX000004) and ground wires (A-M system, Cat. No. 781000), respectively. During surgery, tetrodes and reference wires (200 kΩ - 300 ΩU for tetrodes and 20 kΩ - 30 kΩ for reference wires) were lowered above GC (1.2 mm below the cortical surface). Movable bundles were further lowered 300 μm before the first day of recordings and ~80 μm after each recording session. Tetrodes, ground wires and a head screw (for the purpose of head restraint) were cemented to the skull with dental acrylic (Hygenic Perm Reline, Coltene). Before implantation, tetrodes were coated with a fluorescent dye (DiI; ThermoFisher), which allowed us to verify placement at the end of each experiment (Figure S1A). Animals were allowed to recover for a minimum of 7 days before water restriction regimen and training began.

Taste-based, two-alternative choice task—Once recovered from surgery, mice were water restricted with 1.5 mL water daily for 1 week before training. Mice were head-restrained and trained in a custom-built setup to perform a taste-based 2-AC task, which was inspired by the object location discrimination task [18, 37]. The behavioral setup consisted of one central spout and two lateral spouts. Starting and ending position of the spouts and their speed were controlled by Zaber motors (X-LSM, Zaber) via LabView software. In addition, a movable aspiration line was used to clean the central spout by aspiring residues of the tastant drop after each trial. The central spout consisted of 5 independent metal tubes, each one connected to its taste line. Gustatory stimuli (sucrose [100 mM], maltose [300 mM], quinine [0.5 mM] and sucrose octaacetate [0.5 mM], Sigma-Aldrich) were delivered in ~2 μL droplets by a gravity-based taste delivery system. The lateral spouts consist of two

metal tubes and were used to deliver a drop of water (~3 μL) as reward. The tips of two lateral spouts were spaced 5 mm apart from each other. Licking signals were detected with licking detectors [38], which were activated by the tongue's contact with the metal spouts.

Mice were trained to associate sucrose(S) and quinine (Q) delivered from the central spout with water reward at the left lateral spout, and to associate maltose (M) and sucrose octaacetate (SO) delivered from the central spout with water reward at the right lateral spout. At each trial, the central spout containing a preformed drop of a tastant(pseudo-randomly chosen from S, M, Q and SO) moved close to the mouse, and started to retract once licking to the central spout was detected. This configuration resulted in a short window for sampling (~500 ms). After a delay period (average interval between the last lick for the central spout and the first lick for a lateral spout was 2 s), two lateral spouts advanced, allowing the mouse to make a lateral lick and report the choice. The first lick to either of the lateral spouts was counted as the choice. A correct lateral spout choice triggered a drop of water, while an incorrect choice triggered a time out (5 s) before the onset of the inter-trial interval. A timeout before the inter-trial interval was also triggered if the mouse failed to sample the tastants from the central spout or failed to lick to either one of the two lateral spouts. The inter-trial interval was 6 ± 1 s.

To minimize the influence of non-gustatory cues (valve clicks, odor of tastants) on animal's performance, experimental precautions were adopted. A fan was used to blow away the possible odor of tastants, and constant white noise was played to mask the sound of valve clicks. In addition, control experiments were performed to verify the reliance on gustatory cues in the performance of the task. A group of well-trained mice (> 75% correct choices for more than 3 days in a row; n = 5) was tested in a behavioral session in which gustatory stimuli were replaced with water. Under these conditions, performance dropped to chance level (water versus tastants, 0.530 ± 0.035 versus 0.862 ± 0.031, paired t test, $t_{(4)} = -6.15$, p = 0.003), confirming that taste information was essential to discriminate the four gustatory stimuli.

Electrophysiological recordings—Single units were recorded via a multichannel acquisition processor (MAP data acquisition system, Plexon, Dallas, TX) in mice performing the taste-based 2-AC task. Signals were amplified, bandpass filtered (300–8000 Hz), and digitized at 40 kHz. Extracellular waveforms were isolated by threshold detection and were further sorted and classified as single units using Offline Sorter (Plexon, Dallas, TX). Single units were isolated based on principal component analysis (PCA) (across the four electrodes of each individual tetrode) and identified with distinct clusters in PCA spaces and clear refractory periods (> 1 ms) in autocorrelation histograms. Tetrodes were lowered ~80 μm after each recording session to avoid sampling the same neurons. In total, we recorded 214 neurons from 5 mice in 21 sessions; the average yield was 42.5 neurons per mouse and 10.2 neurons per session.

Chemogenetic manipulation of GC—See section on "Surgical procedures for viral injections, fiber optic cannulae and electrodes implantation" for surgical procedures. Mice with GC neurons infected with hM4Di-mCherry (n = 6) or mCherry (n = 5) were used in these experiments. After learning the task and showing stable performances (correct choices

> 75%) for more than three consecutive days, mice received intraperitoneal (i.p.) injections of saline (10 ml/kg body weight) or clozapine N-oxide (CNO, 10 mg/kg, 10 ml/kg, Sigma). Drugs (saline or CNO) were administered 30–40 minutes prior to the start of the behavioral sessions. CNO was stored at −20°C and dissolved in saline (0.9%) to reach the final concentration (1 mg/ml). CNO doses were chosen based on previously published work [39].

Optogenetic manipulation of GC—See section on "Surgical procedures for viral injections, fiber optic cannulae and electrodes implantation" for surgical procedures. PV-Cre mice with GC neurons infected with DIO-ChR2-EYFP (n = 4) or DIO-EYFP (n = 4) and implanted with tapered fiber optic cannulae were used for these experiments. A 473 nm laser (473 nm, 100 mW DPSS laser system, Opto Engine LLC) was used to deliver the light. Two 470 nm LEDs were placed in front of each mouse, delivering on/off flashes at 20 Hz. LED flashing lights acted as a background masking stimulus for the laser used for photostimulation. Only 30% of the trials were randomly stimulated with the light from the laser (20 Hz, 3~4 mW). For perturbing activity during the sampling epoch, a 1 s long pulsing light (20 Hz) was delivered from 0.5 s before to 0.5 s after the onset of the sampling epoch to activate inhibitory interneurons. For perturbing activity during the delay epoch, photostimulation was delivered for 2 s at the onset of the delay epoch. Each mouse received 2-3 sessions of photostimulation covering the sampling epoch, and 3 sessions of photostimulation during the delay. Sessions with stimulation covering the sampling epoch were alternated with sessions for stimulation during the delay epoch.

Histological staining—Mice were deeply anesthetized with an intraperitoneal injection of ketamine/dexmedetomidine (140 mg/kg, 2 mg/kg) and were intracardially perfused with PBS followed by 4% paraformaldehyde. The brain was post-fixed with 4% paraformaldehyde overnight, cryoprotected with 30% sucrose for 3 days, and was then sectioned with a cryostat into 50 μm coronal slices. For visualizing electrode tracks or expression of AAV constructs, slices were counterstained with Hoechst 33342 (1:5000 dilution, H3570, ThermoFisher, Waltham, MA) using standard techniques.

QUANTIFICATION AND STATISTICAL ANALYSIS

Data analysis was performed using Neuroexplorer (Plexon, Dallas, TX), custom scripts written in MATLAB (MathWorks, Natick, MA), ImageJ (NIH), and Prism 8 (GraphPad).

Behavioral analysis—Task performance was measured as the fraction of correct trials over the total number of correct and error trials. Error trials were defined as trials in which mice licked to the wrong lateral spout. Trials with no licking to the central or lateral spouts were excluded from analysis. Normally these trials occurred at the end of the session. One-way analysis of variance (ANOVA) was used to compare the sampling duration and performance among 4 tastants. A paired t test was used to compare reaction time and duration of lateral licking between left and right trials.

Taste-evoked response—Single unit spike timestamps were aligned to the first lick at the central spout. Perievent rasters of individual units were used to construct perstimulus time histograms (PSTHs, 100 ms bin size). Taste-selective activity was assessed by

examining firing rates averaged across trials and over a 500 ms window after the first central lick. Firing rates in S, M, Q and SO trials were compared using a Kruskal-Wallis test (a neuron was deemed taste selective if $p < 0.05$). Only neurons showing taste selectivity were further analyzed to assess the modulation evoked by a specific tastant. For each tastant, mean firing rates in a 500 ms window after the first lick to the central spout were compared with mean firing rates in a 500 ms window prior to the first lick to the central spout using a Wilcoxon rank sum test (a neuron was deemed responsive to a certain tastant if the $p < 0.01$).

Population decoding of taste information—To characterize the temporal dynamics of gustatory processing in GC, we first applied a population decoder (Neural Decoding Toolbox, http://www.readout.info), based on maximum correlation coefficient [21]. Specifically, neurons recorded across different sessions were used to construct a pseudo population. The results presented are from 181 out of 214 neurons, as only neurons with at least 30 trials for each tastant were used to ensure robustness of classification. The results were confirmed when we relaxed the trial number constraint to 11 and included all neurons (n = 214). Spike timestamps for each neuron were aligned to the first lick of the central spout (time 0) and were binned (bin size = 100 ms) to construct a firing rate matrix, where each row represents a trial and each column represents a bin. The matrix is composed of spikes occurring from time 0 to time 2.5 s. Firing rates were normalized to Z-scores. Data were randomly divided into 10 splits, out of which 9 were used to train the classifier (max correlation coefficient) and the remaining 1 was used to test the classifier. This process was repeated 10 times, each time with different training and testing splits, to compute the decoding accuracy. Decoding accuracy within the 0–0.5 s temporal windows was averaged to represent the decoding accuracy for the sampling epoch. Decoding accuracy within the 0.5–1.5 s and 1.5 – 2.5 s temporal windows were averaged to represent the decoding accuracy during the delay. The decoding procedure was further repeated 10 times to compute the variation of the decoding accuracy for the sampling and delay epoch. In addition to the decoding accuracy, confusion matrices within 0–0.5 s, 0.5–1.5 s and 1.5–2.5 s temporal windows were also computed. The following procedures were performed to infer statistical differences in decoding performance for tastants associated with the same action. We first randomly shuffled firing rates within each time bin (100 ms) for the sampling and delay epochs, then we ran the population decoder on the shuffled data. We repeated this step 1000 times to calculate the confusion matrices for sampling (0–0.5 s), early delay (0.5–1.5 s) and late delay (1.5–2.5 s) periods at each iteration. Null distribution of the difference in confusion for tastants associated with the same action (i.e., confusion between S and Q, or between M and SO) between different epochs (i.e., late delay versus sampling, late delay versus early delay) was computed based on the shuffled data. The difference in confusion of tastants associated with the same action from the actual data was compared to the null distribution (permutation test, p value was calculated as the proportion of cases where shuffled data has an equal or bigger difference than the real data). We found that the confusion between tastants associated with the same action was significantly larger during the late delay period compared to sampling or early delay periods ($p < 0.001$, permutation test).

Visualization of population activity with principal component analysis (PCA)— To visualize population activity over time, we applied PCA. Specifically, neurons recorded across different sessions (n = 214) were used to construct a pseudo population. For each neuron, spike timestamps were aligned to the first lick of the central spout (time 0) and PSTHs were computed (bin size = 100 ms, window = 0–2.5 s). A firing rate matrix was constructed for the pseudo population, where each row represents a bin and each column represents a neuron. We used PCA to find the principal component coefficients of the matrix, and applied the coefficients to the population activity evoked by S, Q, M, and SO. Population activity was projected onto the PC space. Only the first 3 PCs were used for visualization and analysis. PCA results were confirmed also when the analysis was performed exclusively on neurons with at least 30 trials for each tastant (n = 181).

Pairwise distance between taste-evoked activity— To calculate the pairwise distance between taste-evoked activity, we applied a receiver operator characteristic (ROC) analysis for each single unit (n = 214). Single unit spike timestamps were aligned to the first lick of the central spout and PSTHs were constructed (bin size is 100 ms) for the 4 different tastants. The area under the ROC curve (auROC) was used to compute the auROC distance in neural activity between a pair of tastants: $\text{auROC\_D}_{\text{tastant-pair}} = |\ 2 \times (\text{auROC} - 0.5)\ |$, ranging from 0 to 1, where 0 represents similar firing and 1 represents different firing for the pair of tastants. Distance in neural activity evoked by tastant-pairs associated with the same actions was computed as: $\text{Distance} = \frac{1}{2} \times (\text{auROC\_D}_{\text{S-Q}} + \text{auROC\_D}_{\text{M-SO}})$; and distance in neural activity evoked by tastant-pairs with same qualities was computed as: $\text{Distance} = \frac{1}{2} \times (\text{auROC\_D}_{\text{S-M}} + \text{auROC\_D}_{\text{Q-SO}})$. The results were confirmed when we only analyzed neurons with at least 30 trials for each tastant (n = 181). Distance in neural activity evoked by tastant-pairs associated with the same actions or the same qualities was compared via two-way ANOVA with post hoc Bonferroni's multiple comparisons test (p < 0.05).

Preparatory activity during the delay epoch— Preparatory activity was first assessed only in correct trials. Single unit spike timestamps were aligned to the first lick of the lateral spout and PSTHs were constructed (bin size is 100 ms). ROC analysis [17, 22] was then used to compare mean firing rates between left and right correct trials in a 1 s window before the first lateral lick. Specifically, the area under the ROC curve (auROC) was used to calculate the direction index as: direction index = $2 \times (\text{auROC} - 0.5)$. Direction index ranged from −1 to −1, where 1 means higher firing rate in left trials (see Neuron #1 in Figure 3B), 1 means higher firing rate in right trials (see Neuron #2 in Figure 3B) and 0 means similar firing rate between left and right trials. To assess the significance of direction index, we used a permutation test where left/right correct trials were shuffled without replacement. Data were shuffled 1000 times and the pseudo direction index was calculated for each iteration of the shuffling. The p value was computed by comparing the actual direction index with the pseudo index. We used a criteria p < 0.01 to determine significance. Neurons with significant direction index during the delay were defined as preparatory neurons, and the activity during the delay was deemed as preparatory activity. To assess the tuning of the preparatory neurons, we measured the change of preparatory firing rates (i.e., firing rate in 1 s before decision) relative to background firing (i.e., firing rate in 2 s prior to taste delivery)

(Figure S2A). We found that 32% (29/89) of the neurons decreased their firing rate while 37% (33/89) increased their firing rate for both left and right rewarded trials. Conversely, 30% (27/89) of the preparatory neurons displayed incongruent firing (i.e., increased firing rate for one direction and decreased firing rate for the other). In addition, we computed the direction-preference tuning profile of the preparatory neurons comparing the absolute change in firing rates between left and right rewarded trials. Direction preference was then determined based on the trial type (left or right) that showed the largest change in absolute firing rate change. With this method, we found that 18.2% of neurons had left direction preference (left preferring) and 23.4% had right direction preference (right preferring; Chi-square test, (1) = 1.7, p = 0.19; Figure S2B).

Preparatory neurons were further analyzed to extract information about taste selectivity. For assessing taste selectivity, we compared activity between S and Q trials (left trials), or activity between M and SO trials (right trials) during either sampling or late delay epochs (1 s before first lateral lick). We used a similar ROC analysis to quantify taste selectivity, calculated as: taste selectivity = $| 2 \times (auROC-0.5) |$, ranging from 0 to 1, where 0 represents no selectivity between tastants (similar firing rates between S and Q trials, or between M and Q trials) and 1 represents high selectivity between tastants. We used the same permutation procedure described above to test for significance of taste response selectivity. A neuron was deemed to be taste-selective during the delay epoch if it showed either significant selectivity between S and Q or between M and SO trials. To compare taste selectivity and direction index for each neuron, the maximum selectivity between the two pair of tastants was used (Figures 3F and S2D).

Classification of correct and error trials—To analyze the relationship between preparatory activity and actions, we applied the population decoder mentioned above to the classification of correct and error trials (i.e., distinguishing left-cued correct trials from left-cued incorrect trials, and right-cued correct trials from right-cued incorrect trials). Preparatory neurons recorded across sessions (49 out of 89 neurons, only neurons with at least 10 error trials for both left and right trials were used) were grouped to construct a pseudo population. Spike timestamps for each neuron were aligned to the first lick of the lateral spout (time 0) and binned (bin size = 100 ms) to construct a firing rate matrix, where each row represents a trial and each column represents a bin. The matrix was composed of spikes occurring from time −2 to time 1 s. Firing rates were normalized to Z-scores. Data were randomly divided into 10 splits, out of which 9 splits were used to train the classifier (max correlation coefficient) and the remaining 1 split was used for testing it. This process was repeated 10 times, each time with different training and testing splits, to compute classification accuracy. We first applied the decoder trained with left-cued (S and Q) trials (including same number of correct and error trials) to classify whether left-cued trials were correct or incorrect. We then applied the decoder trained with right-cued (M and SO) trials (including same number of correct and error trials) to classify the right-cued correct/error trials. The overall classification accuracy of correct/error trials was represented as the averaged classification accuracy calculated for S/Q trials and M/SO trials. To evaluate whether classification accuracy was above chance, we first shuffled the labels for correct and error trials, then trained the decoder on shuffled data to compute the null distribution of

classification accuracy. Classification accuracy with $p < 0.001$ was deemed significantly different from the chance (Figure 3G, gray bar).

In addition, we calculated the direction index for error trials. Preparatory neurons with at least 10 error trials for both left and right trials (49 out of 89 neurons) were included in this analysis. We used the same permutation test described above to calculate the significance of direction index in error trials. In total, 12 out of 49 (24.49%) preparatory neurons show significant direction index in error trials (red dots in Figure 3H).

Analysis of the orofacial movements—Oro-motor activity was recorded at a rate of 30 frames per second with a camera placed in front of the mouse face (Video S1). Images were acquired and synchronized with recording of neural activity by Cineplex software (Plexon, Dallas, TX) and imported in MATLAB for offline analysis. Only videos of orofacial movements from sessions where neurons showed a direction index significantly different from 0 (16 sessions) were included in this analysis. Movements of the orofacial region for each mouse were assessed by frame-by-frame video analysis [12,13]. Briefly, a region of interest (ROI) was drawn around the animal's mouth, avoiding the lateral spouts. Then we computed the absolute difference of the average pixel intensity of the entire ROIs across consecutive frames around the first lateral lick (time 0, Figures S3A and S3B). Changes in pixel intensity values of the orofacial region were normalized to background changes in pixel intensity obtained from a second ROI drawn away from the orofacial region. This allowed us correcting for changes due to fluctuations in background light intensity. Orofacial movement was represented as change in pixel intensity. We applied the same ROC analysis described above to compute the direction index based on the change in pixel intensity in left and right correct trials. Significance of the direction index was inferred with the permutation test described above. To analyze the directionality of preparatory tongue protrusions, the ROI around the animal's mouth was divided into two halves (ROI_{left} and ROI_{right}). Orofacial movements within both ROIs were then extracted using the same method described above for left and right correct trials in each experimental session (16 sessions). In order to represent the directionality of tongue protrusion, we computed the time-course difference of orofacial movements between the two halves ROIs (the orofacial movements extracted from ROI_{left} were subtracted from the ones extracted from ROI_{right} as [ROI_{left} - ROI_{right}]) for left and right rewarded trials (Figure S3F). Two-way ANOVA with post hoc Bonferroni's multiple comparisons test ($p < 0.05$) was then used to statistically infer the significant differences in direction tongue protrusion in left and right trials.

Analysis of Chemogenetic/Optogenetic manipulation of GC—For chemogenetic manipulation of GC, a two-way repeated-measures ANOVA (mix-effect ANOVA) was conducted on the effect of two factors (hM4Di versus mCherry, saline versus CNO [repeated-measures]) on behavioral performance, sampling duration, and reaction time. For optogenetic manipulation of GC, a two-way repeated-measures ANOVA (mix-effect ANOVA) was conducted on the effect of two factors (ChR2 versus EYFP, no light versus light [repeated-measures]) on the behavioral performance, sampling duration, and reaction time.

DATA AND CODE AVAILABILITY

Datasets and code supporting the current study are deposited and available in the Mendeley Data (https://doi.org/10.17632/n2hkg6tcsm.1) and Github repository (https://github.com/fontaninilab/currentbiology_2020), respectively.

Supplementary Material

Refer to Web version on PubMed Central for supplementary material.

ACKNOWLEDGMENTS

REFERENCES

1. Spector AC, and Travers SP (2005). The representation of taste quality in the mammalian nervous system. Behav. Cogn. Neurosci. Rev 4, 143–191. [PubMed: 16510892]

2. Carleton A, Accolla R, and Simon SA (2010). Coding in the mammalian gustatory system. Trends Neurosci. 33, 326–334. [PubMed: 20493563]

3. Maffei A, Haley M, and Fontanini A (2012). Neural processing of gustatory information in insular circuits. Curr. Opin. Neurobiol 22, 709–716. [PubMed: 22554880]

4. Vincis R, and Fontanini A (2016). A gustocentric perspective to understanding primary sensory cortices. Curr. Opin. Neurobiol 40, 118–124. [PubMed: 27455038]

5. Grossman SE, Fontanini A, Wieskopf JS, and Katz DB (2008). Learning-related plasticity of temporal coding in simultaneously recorded amygdala-cortical ensembles. J. Neurosci 28, 2864–2873. [PubMed: 18337417]

6. Katz DB, Simon SA, and Nicolelis MA (2001). Dynamic and multimodal responses of gustatory cortical neurons in awake rats. J. Neurosci 21, 4478–4489. [PubMed: 11404435]

7. Sadacca BF, Rothwax JT, and Katz DB (2012). Sodium concentration coding gives way to evaluative coding in cortex and amygdala. J. Neurosci 32, 9999–10011. [PubMed: 22815514]

8. Maier JX (2017). Single-neuron responses to intraoral delivery of odor solutions in primary olfactory and gustatory cortex. J. Neurophysiol 117, 1293–1304. [PubMed: 28003413]

9. Saddoris MP, Holland PC, and Gallagher M (2009). Associatively learned representations of taste outcomes activate taste-encoding neural ensembles in gustatory cortex. J. Neurosci 29, 15386–15396. [PubMed: 20007463]

10. Samuelsen CL, and Fontanini A (2017). Processing of intraoral olfactory and gustatory signals in the gustatory cortex of awake rats. J. Neurosci 37, 244–257. [PubMed: 28077705]

11. Samuelsen CL, Gardner MP, and Fontanini A (2012). Effects of cuetriggered expectation on cortical processing of taste. Neuron 74, 410–422. [PubMed: 22542192]

12. Vincis R, and Fontanini A (2016). Associative learning changes crossmodal representations in the gustatory cortex. eLife 5, e16420. [PubMed: 27572258]

13. Gardner MP, and Fontanini A (2014). Encoding and tracking of outcome-specific expectancy in the gustatory cortex of alert rats. J. Neurosci 34, 13000–13017. [PubMed: 25253848]

14. Kusumoto-Yoshida I, Liu H, Chen BT, Fontanini A, and Bonci A (2015). Central role for the insular cortex in mediating conditioned responses to anticipatory cues. Proc. Natl. Acad. Sci. USA 112, 1190–1195. [PubMed: 25583486]

15. Livneh Y, Ramesh RN, Burgess CR, Levandowski KM, Madara JC, Fenselau H, Goldey GJ, Diaz VE, Jikomes N, Resch JM, et al. (2017). Homeostatic circuits selectively gate food cue responses in insular cortex. Nature 546, 611–616. [PubMed: 28614299]

16. Mukherjee N, Wachutka J, and Katz DB (2019). Impact of preciselytimed inhibition of gustatory cortex on taste behavior depends on single-trial ensemble dynamics. eLife 8, e45968. [PubMed: 31232693]

17. Fonseca E, de Lafuente V, Simon SA, and Gutierrez R (2018). Sucrose intensity coding and decision-making in rat gustatory cortices. eLife 7, e41152. [PubMed: 30451686]

18. Guo ZV, Li N, Huber D, Ophir E, Gutnisky D, Ting JT, Feng G, and Svoboda K (2014). Flow of cortical activity underlying a tactile decision in mice. Neuron 81, 179–194. [PubMed: 24361077]

19. Yamamoto T, Yuyama N, Kato T, and Kawamura Y (1984). Gustatory responses of cortical neurons in rats. I. Response characteristics. J. Neurophysiol 51, 616–635. [PubMed: 6716115]

20. Yamamoto T, Yuyama N, Kato T, and Kawamura Y (1985). Gustatory responses of cortical neurons in rats. II. Information processing of taste quality. J. Neurophysiol 53, 1356–1369. [PubMed: 4009223]

21. Meyers EM (2013). The neural decoding toolbox. Front. Neuroinform 7, 8. [PubMed: 23734125]

22. Feierstein CE, Quirk MC, Uchida N, Sosulski DL, and Mainen ZF (2006). Representation of spatial goals in rat orbitofrontal cortex. Neuron 51, 495–507. [PubMed: 16908414]

23. Musall S, Kaufman MT, Juavinett AL, Gluf S, and Churchland AK (2019). Single-trial neural dynamics are dominated by richly varied movements. Nat. Neurosci 22, 1677–1686. [PubMed: 31551604]

24. Makino H, Ren C, Liu H, Kim AN, Kondapaneni N, Liu X, Kuzum D, and Komiyama T (2017). Transformation of cortex-wide emergent properties during motor learning. Neuron 94, 880–890.e8. [PubMed: 28521138]

25. Allen WE, Kauvar IV, Chen MZ, Richman EB, Yang SJ, Chan K, Gradinaru V, Deverman BE, Luo L, and Deisseroth K (2017). Global representations of goal-directed behavior in distinct cell types of mouse neocortex. Neuron 94, 891–907.e6. [PubMed: 28521139]

26. Armbruster BN, Li X, Pausch MH, Herlitze S, and Roth BL (2007). Evolving the lock to fit the key to create a family of G protein-coupled receptors potently activated by an inert ligand. Proc. Natl. Acad. Sci. USA 104, 5163–5168. [PubMed: 17360345]

27. Estebanez L, Hoffmann D, Voigt BC, and Poulet JFA (2017). Parvalbumin-expressing GABAergic neurons in primary motor cortex signal reaching. Cell Rep. 20, 308–318. [PubMed: 28700934]

28. Roux L, Stark E, Sjulson L, and Buzsá ki G (2014). In vivo optogenetic identification and manipulation of GABAergic interneuron subtypes. Curr. Opin. Neurobiol 26, 88–95. [PubMed: 24440414]

29. Sparta DR, Hovelsø N, Mason AO, Kantak PA, Ung RL, Decot HK, and Stuber GD (2014). Activation of prefrontal cortical parvalbumin interneurons facilitates extinction of reward-seeking behavior. J. Neurosci 34, 3699–3705. [PubMed: 24599468]

30. Li JX, Maier JX, Reid EE, and Katz DB (2016). Sensory cortical activity is related to the selection of a rhythmic motor action pattern. J. Neurosci 36, 5596–5607. [PubMed: 27194338]

31. Levitan D, Lin JY, Wachutka J, Mukherjee N, Nelson SB, and Katz DB (2019). Single and population coding of taste in the gustatory cortex of awake mice. J. Neurophysiol 122, 1342–1356. [PubMed: 31339800]

32. Gallo M, Roldan G, and Bures J (1992). Differential involvement of gustatory insular cortex and amygdala in the acquisition and retrieval of conditioned taste aversion in rats. Behav. Brain Res. 52, 91–97. [PubMed: 1335264]

33. Peng Y, Gillis-Smith S, Jin H, Tra￿nkner D, Ryba NJ, and Zuker CS (2015). Sweet and bitter taste in the brain of awake behaving animals. Nature 527, 512–515. [PubMed: 26580015]

34. Liu H, and Fontanini A (2015). State dependency of chemosensory coding in the gustatory thalamus (VPMpc) of alert rats. J. Neurosci 35, 15479–15491. [PubMed: 26609147]

35. Weiss MS, Victor JD, and Di Lorenzo PM (2014). Taste coding in the parabrachial nucleus of the pons in awake, freely licking rats and comparison with the nucleus of the solitary tract. J. Neurophysiol 111, 1655–1670. [PubMed: 24381029]

36. Pisanello F, Mandelbaum G, Pisanello M, Oldenburg IA, Sileo L, Markowitz JE, Peterson RE, Della Patria A, Haynes TM, Emara MS, et al. (2017). Dynamic illumination of spatially restricted or large brain volumes via a single tapered optical fiber. Nat. Neurosci 20, 1180–1188. [PubMed: 28628101]

37. Guo ZV, Hires SA, Li N, O'Connor DH, Komiyama T, Ophir E, Huber D, Bonardi C, Morandell K, Gutnisky D, et al. (2014). Procedures for behavioral experiments in head-fixed mice. PLoS ONE 9, e88678. [PubMed: 24520413]

38. Slotnick B (2009). A simple 2-transistor touch or lick detector circuit. J. Exp. Anal. Behav 91, 253–255. [PubMed: 19794837]

39. Farrell MS, and Roth BL (2013). Pharmacosynthetics: reimagining the pharmacogenetic approach. Brain Res. 1511, 6–20. [PubMed: 23063887]

Author Manuscript

Author Manuscript

Author Manuscript

Author Manuscript

Highlights

- Mice learn a task where taste sampling and action are separated by a delay period

- Gustatory cortex (GC) neurons encode task-related signals during the delay period

- Manipulation of GC activity during the delay period impacts behavioral performance

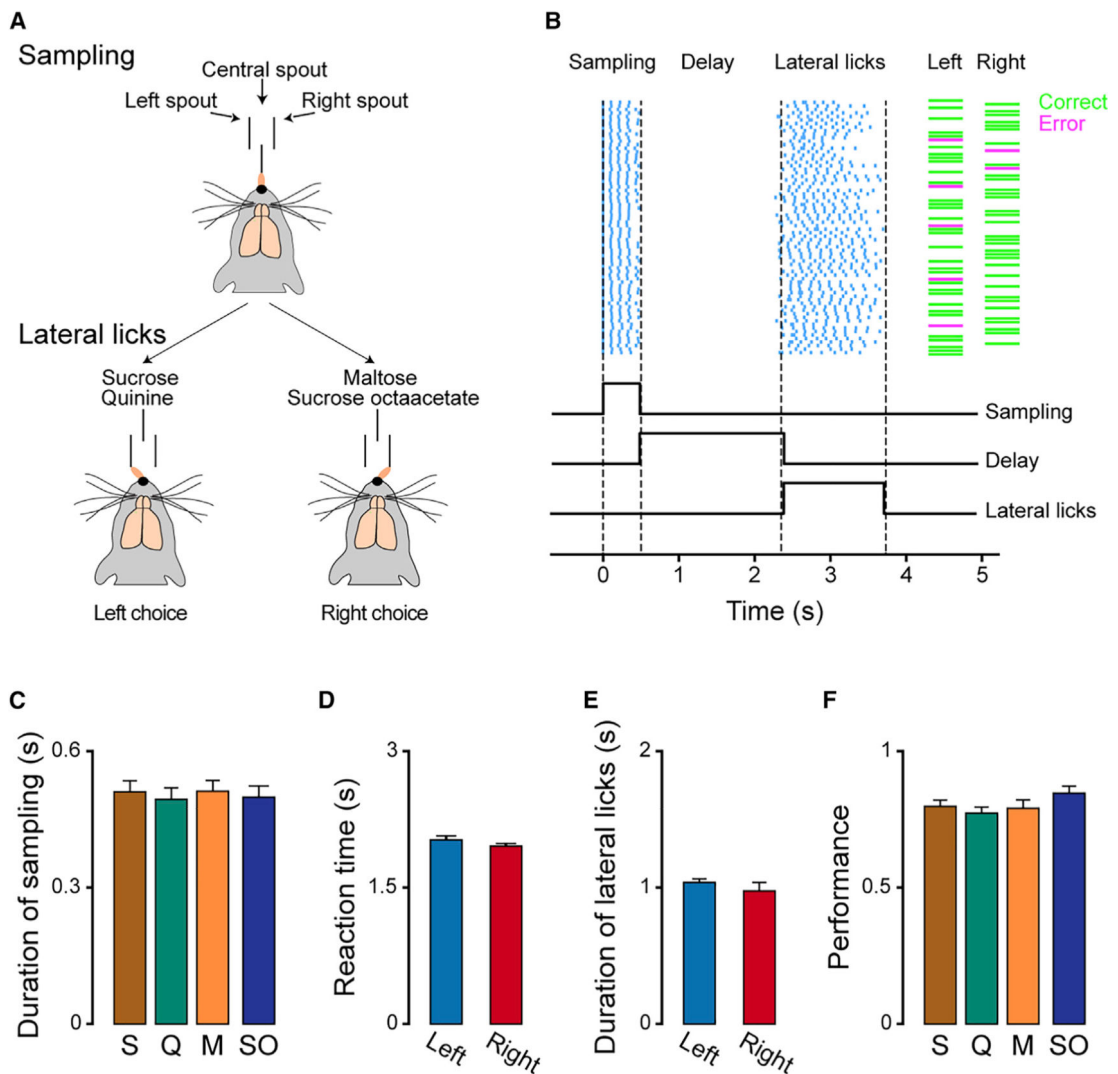- GC is responsible of sensorimotor transformation in a taste decision-making task

Figure 1. Taste-Based, Two-Alternative Choice Task

(A) Diagram showing a head-fixed mouse sampling tastants from a central spout and responding with appropriate licking.

(B) Top panel: representative raster plots of licking activity during a behavioral session. Each row represents a single trial, and each cyan tick represents a lick. Thegreen horizontal bars represent correct trials, and the magenta horizontal bars represent errors. Bottom panel: schematic diagram of the taste-based, 2-AC with its three epochs is shown: sampling; delay; and lateral licks.

(C) Bar plots showing the average duration of taste sampling (i.e., how long mice licked to the central spout during the sampling epoch) for each stimulus (M,maltose; Q, quinine; S, sucrose; SO, sucrose octaacetate). Error bars represent standard error of the mean (SEM).

(D) Bar plots showing the average reaction time from the end of taste sampling to the first lateral lick for left (blue) and right (red) trials. Error bars represent SEM.

(E) Bar plots showing the duration of lateral licks for left (blue) and right (red) correct trials. Error bars represent SEM.

(F) Bar plots showing the average of behavioral performance (fraction of correct choices) for the four gustatory stimuli.

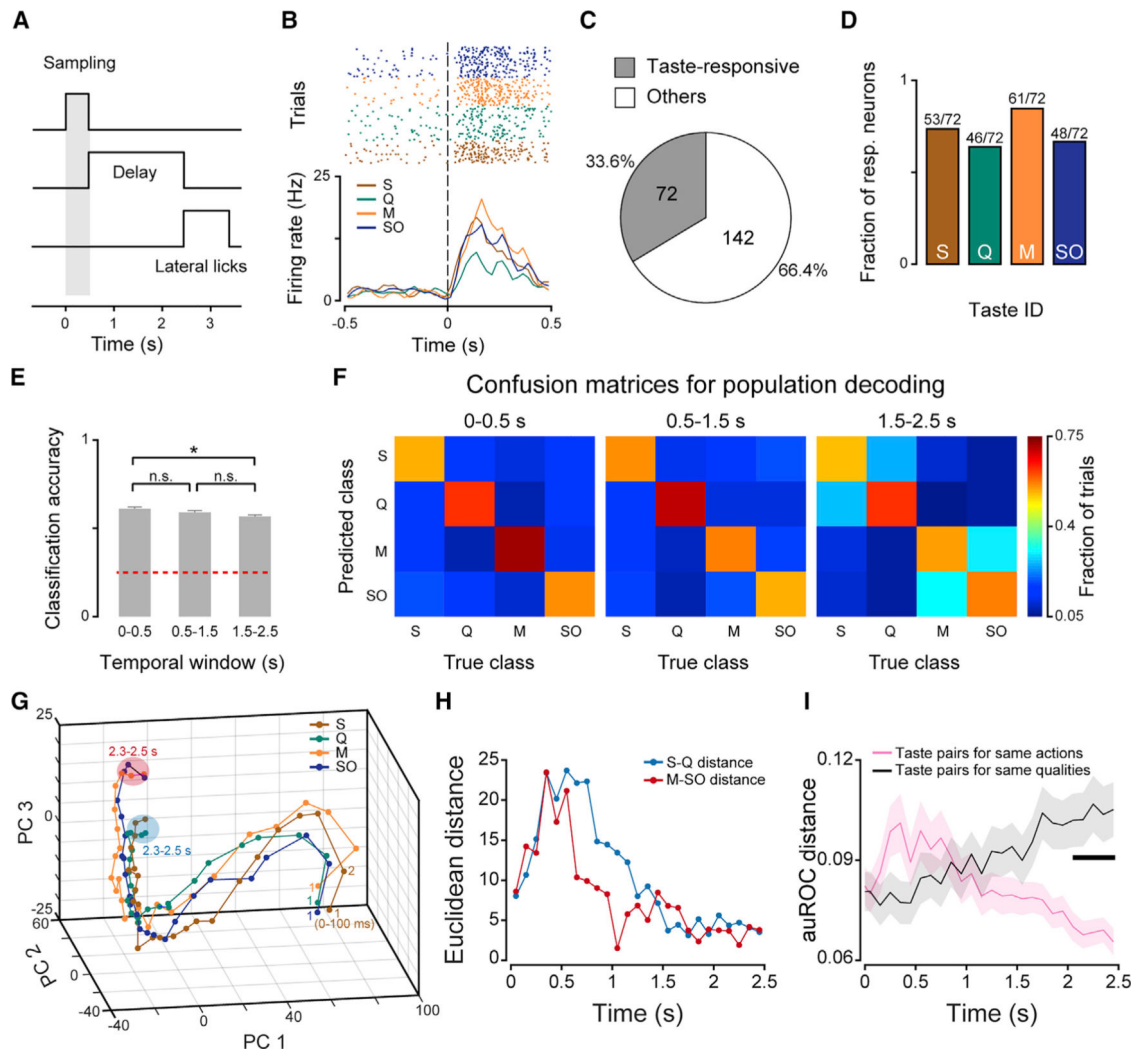In (C)–(F) bar plots (n = 16 mice), error bars represent SEM.

Figure 2. Taste Representation in GC

(A) Schematic showing the trial structure. The gray bar represents the 500-ms long sampling epoch. Time 0 represents the first lick to the central spout.

(B) Raster plot and PSTH for a representative neuron showing responses to the four taste stimuli. Dashed lines at time 0 represent the first lick to the central spout.

(C) (C) Pie chart showing the proportion of taste-responsive (gray) and non-responsive (white) neurons. Criterion for taste responsiveness: Kruskal-Wallis test, $p < 0.05$, followed by a Wilcoxon rank sum test, $p < 0.01$; see STAR Methods.

(D) Bar plots showing the fraction of taste-responsive neurons modulated by each of the four gustatory stimuli used.

(E) Bar plots showing population decoding accuracy for three different temporal windows. Time 0 is the first lick to the central spout. Temporal window from 0 to 0.5 s: sampling epoch; windows from 0.5 to 1.5 s and 1.5 to 2.5 s: delay epoch. Bars represent the mean, and error bars represent SEM. One-way ANOVA and post hoc Tukey's HSD test; *$p < 0.5$; n.s. indicates not significant.

(F) Confusion matrix showing decoding performance for each tastant in the three different temporal windows (left, 0–0.5 s; middle, 0.5–1.5 s; right, 1.5–2.5 s). (G) Trajectories of population activity in PC space for responses to each of the 4 gustatory stimuli. "1" represents the first bin (i.e., 0–100 ms) following the first lick to the central spout. The blue- and red-shaded areas highlight the convergence at the end of the delay (2.3–2.5 s) of S/Q-evoked activity and M/SO-evoked activity, respectively.

(H) Temporal profiles of Euclidean distance in PC space. Blue curve, Euclidean distance between S- and Q-evoked trajectories; red curve, Euclidean distancebetween M and SO-evoked trajectories.

(I) Time course of pairwise difference in firing responses for different tastants. The magenta trace shows the average distance for pairs of tastants associated withthe same actions. The black trace shows the average distance for pairs of tastants associated with same qualities. Shading represents SEM. The thick horizontal black bar represents times at which the distance is significantly different across the two groups (two-way ANOVA; main effect: tastants associated with the same actions versus same qualities, $F(1,10650) = 25.5$, $p < 0.001$; interaction: $F(24,10650) = 4.1$, $p < 0.001$; post hoc Bonferroni's multiple comparisons test, adjust $p < 0.05$).
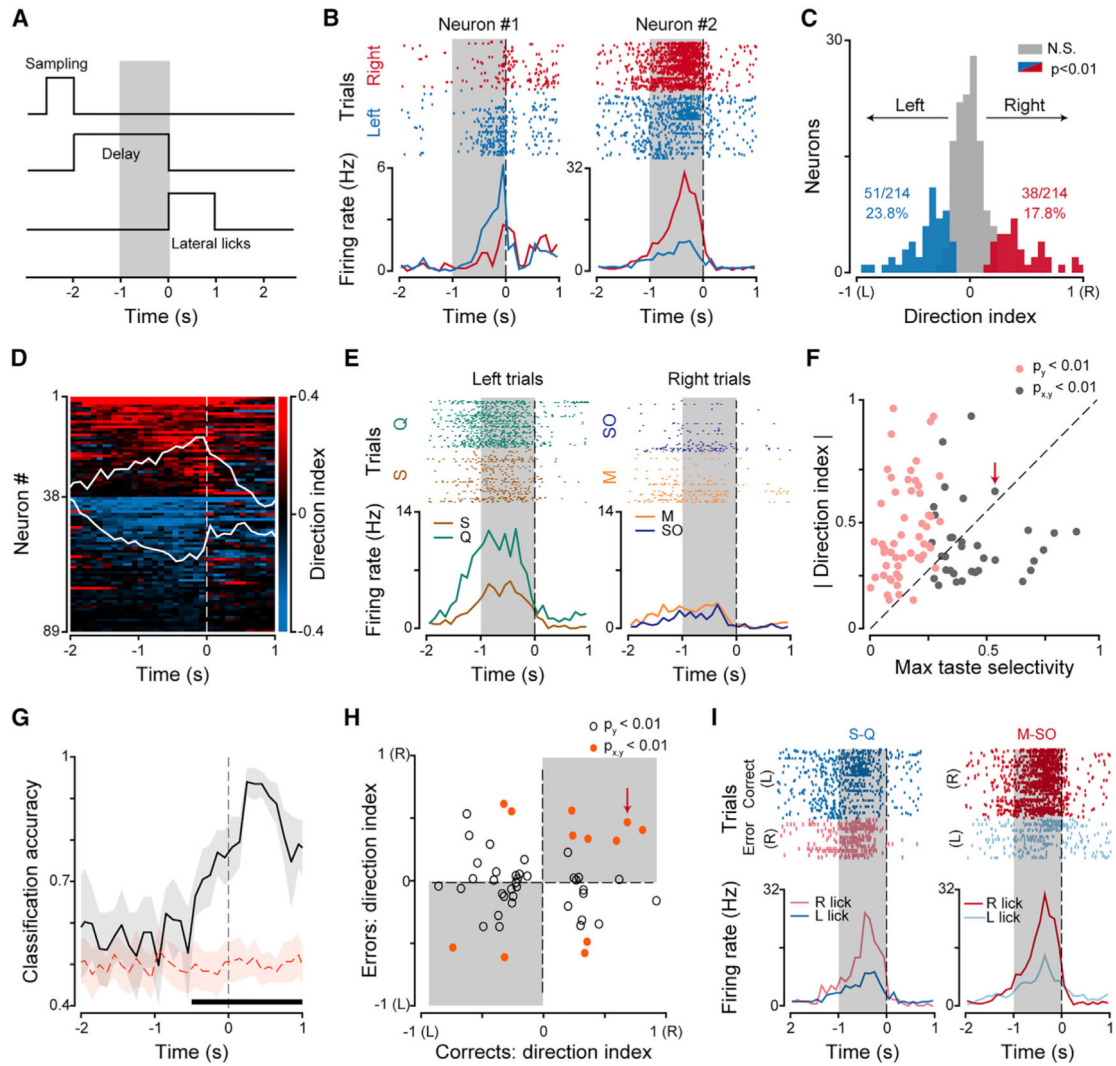
See also Figure S2.

Figure 3. Preparatory Activity in GC

(A) Schematic of trial structure. The gray bar highlights the temporal window (1 s) used to analyze preparatory activity. Time 0 represents the first lick to the lateralspout.

(B) Raster plots and PSTHs of two representative neurons showing direction-selective, preparatory activity. The neuron on the left (neuron no. 1) displays higherfiring rates during the delay period preceding left licks (blue ticks and blue line for raster plot and PSTH, respectively); the neuron on the right (neuron no. 2) displays higher firing rates in anticipation of right licks (red ticks and red line for raster plot and PSTH, respectively). Time 0 represents the first lick to the lateral spout.

(C) Histogram of direction index during the delay epoch. Blue and red bars represent neurons with a direction index significantly <0 or >0, respectively. Gray barsrepresent neurons with no significant direction index (similar firing rate between left and right correct trials).

(D) Heatmap showing the time course of the direction index. Each row represents a single neuron (only neurons with significant direction index are shown). Time0 is the first lick to the lateral spout. Blue and red represent negative (leftward) and positive (rightward)

direction indices. White traces superimposed on the heatmap represent the average direction index for neurons with negative (bottom) and positive direction index (up).

(E) Raster plots and PSTHs for one neuron showing preparatory activity and taste selectivity during the delay epoch. On the left (left trials), raster plot and PSTH for S (brown) and Q (green) trials is shown; on the right (right trials), raster plot and PSTH for M (gold) and SO (blue) trials is shown. Time 0 is the first lick to the lateral spout.

(F) Scatterplot showing the relationship between max taste selectivity and the absolute value of direction index. Each dot (pink and gray) represents a neuron withsignificant direction index ($p_y < 0.01$); gray dots represent neurons that also show taste selectivity during the delay epoch ($p_{x,y} < 0.01$). The gray dot with the red arrow represents the neuron shown in (E).

(G) Time course of classification accuracy for correct and error trials (black curve). Time 0 represents the first lick to the lateral spout. The red dashed curverepresents classification accuracy at chance level when the correct/error trials are shuffled. The thick horizontal black bar represents times with classification accuracy that is significantly higher than chance level (permutation test; $p < 0.001$). Shading represents the 99.5% confidence interval.

(H) Scatterplot showing direction index in correct and error trials. Each dot represents a neuron with significant direction index in correct trials. Orange points represent neurons that also show significant direction index in error trials. Gray-shaded areas highlight the quadrants in which neurons have direction indices with the same sign in correct and error trials, regardless of the gustatory cue. The red arrow indicates the neuron shown in (I).

(I) Raster plots and PSTHs for neuron no. 2 in (B), showing direction indices with the same sign in correct and error trials. Time 0 is the first lick to the lateral spout.Left: raster plots and PSTHs for correct (left licks, dark blue) and error (right lick, light red) trials in response to S and Q are shown. Right: activity for correct (right lick, dark red) and error (left licks, light blue) trials in response to M and SO are shown.
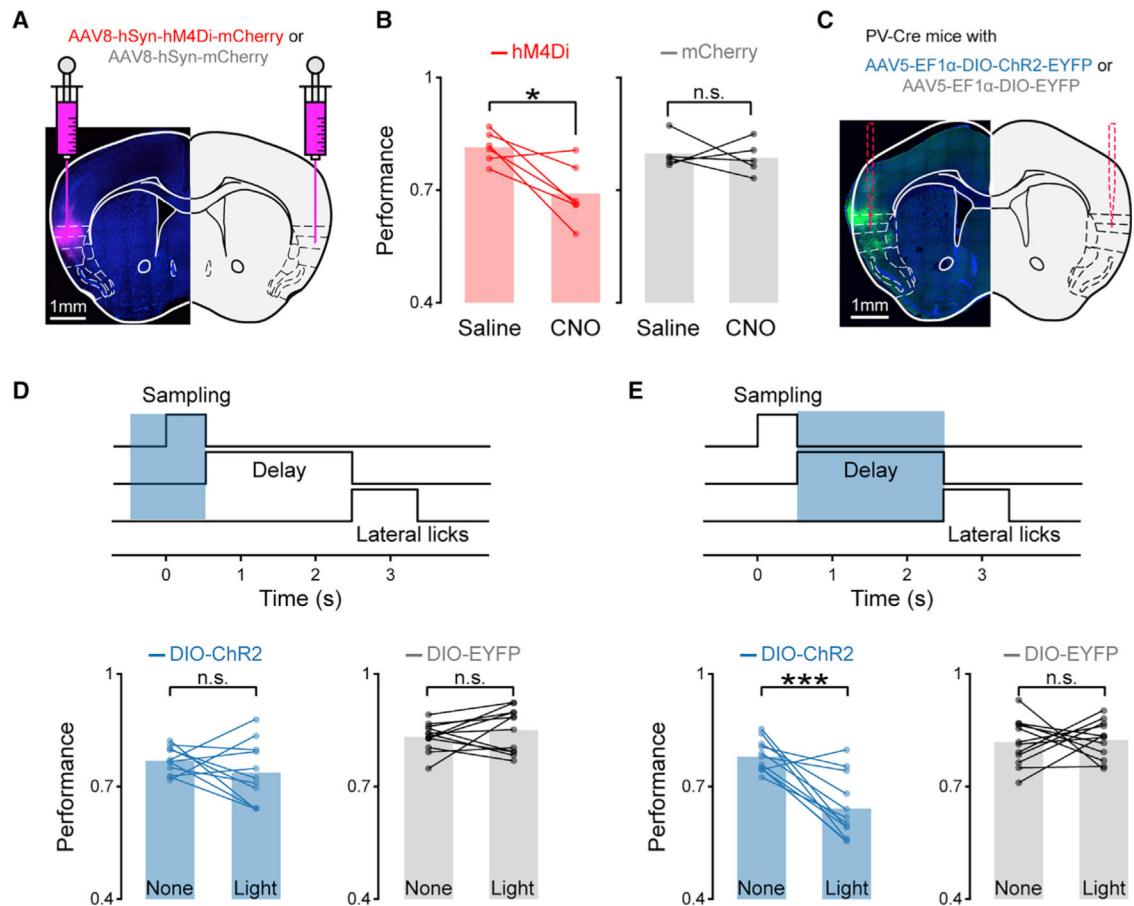
See also Figures S2 and S3.

Figure 4. Behavioral Effects of GC Silencing

(A) Sample histological section showing expression of hM4Di-mCherry (magenta) in GC.

(B) Behavioral performance (fraction of correct trials) after an intraperitoneal (i.p.) injection of saline or CNO in mice with hM4Di-mCherry expression in GC (left,red; n = 6) and only with mCherry expression in GC (right, gray; n = 5). Bar plots, mean value of the performance. Two-way ANOVA; post hoc Bonferroni's multiple comparisons test; *p < 0.05.

(C) Sample histological section showing the expression of ChR2-EYFP (green) in GC and the track of the tapered fiber optic cannula.

(D) Top panel: schematic of trial structure and period of photostimulation (1 s, covering the sampling epoch). Bottom panel: behavioral performance without and with light stimulation in PV-Cre mice injected in GC with ChR2-EYFP (left, blue; 11 animal-session pairs) and with a control construct (EYFP; right, gray; 12 animal-session pairs) is shown. Bar plots, mean value of the performance. Two-way ANOVA.

(E) Top panel: schematic of trial structure and period of the photostimulation (2 s long, covering the delay epoch). Bottom panel: behavioral performance inexperimental (left, blue; 12 animal-session pairs) and control PV-Cre mice (right, gray; 12 animal-session pairs) is shown. Bar plots represent the mean value of the performance. Two-way ANOVA; post hoc Bonferroni's multiple comparisons test; ***p < 0.001.

See also Figures S1 and S4.

KEY RESOURCES TABLE

REAGENT or RESOURCE	SOURCE	IDENTIFIER
Bacterial and Virus Strains		
AAV8-hSyn-hM4Di-mCherry	UNC/Duke vector core	N/A
AAV8-hSyn-mCherry	Duke vector core	N/A
AAV5-EF1α-double floxed-hChR2(H134R)-EYFP-WPRE-HGHpA	A gift from Karl Deisseroth	Addgene AAV5; 20298-AAV5
AAV5-EF1α-DIO-EYFP	A gift from Karl Deisseroth	Addgene AAV5; 27056-AAV5
Chemicals, Peptides, and Recombinant Proteins		
Clozapine N-oxide	Sigma-Aldrich	Cat#: C0832
Sucrose octaacetate	Sigma-Aldrich	Cat#: W303801
Maltose	Sigma-Aldrich	Cat#: M5895
Quinine	Sigma-Aldrich	Cat#: Q1125
Deposited Data		
All data	The current study	http://dx.doi.org/10.17632/n2hkg6tcsm.1
Experimental Models: Organisms/Strains		
Mouse; C57BL/6	Charles River Laboratory	N/A
Mouse; B6. PV-Cre	The Jackson Laboratory	JAX: 017320
Software and Algorithms		
MATLAB	The MathWorks	https://www.mathworks.com/products/matlab.html
The Neural Decoding Toolbox	The neural decoding toolbox [21]	http://www.readout.info/
Offline Sorter v4	Plexon Inc	https://plexon.com/products/offline-sorter/
NeuroExplorer	Nex Technologies	https://www.neuroexplorer.com/
GraphPad Prism 8	GraphPad	https://www.graphpad.com/scientific-software/prism/
Fiji(ImageJ)	NIH	https://imagej.net/Fiji